

## Decomposition in Multi-component AlCoCrCuFeNi High Entropy Alloy

S. Singh<sup>a</sup>, N. Wanderka<sup>\*a</sup>, B.S. Murty<sup>b</sup>, U. Glatzel<sup>c</sup> and J. Banhart<sup>a</sup>

<sup>a</sup>Helmholtz Centre Berlin for Materials and Energy, Hahn-Meitner-Platz, 14109 Berlin, Germany.

<sup>b</sup>Department of Metallurgical and Materials Engineering, Indian Institute of Technology Madras, Chennai -36, India

<sup>c</sup>Metallic and Alloys, University Bayreuth, Ludwig-Thoma Str. 36b, 95447 Bayreuth.

### Abstract

The decomposition behaviour of equiatomic high entropy AlCoCrCuFeNi alloy produced by splat quenching and casting is investigated by analytical high resolution methods such as transmission electron microscopy and 3 dimensional atom probe. The microstructure of splat-quenched alloy shows the formation of only single bcc partially ordered solid solution phase whereas the as-cast alloy forms several phases of cubic crystal structure. The as-cast alloy decomposes into dendrites (bcc) and interdendrites (Cu-rich, fcc-L1<sub>2</sub>). Plates mainly enriched in Ni-Al embedded in solid solution Cr-Fe-Co rich matrix are the dominant features of dendrites. However, Cu-rich phases (plate-like, spherical and rhombohedron-shaped) could also be found in the dendrites. The local compositional analysis of dendrite matrix by atom probe indicates that the alloying elements are not randomly distributed. Moreover, they segregate and form areas with

---

\* Corresponding author Address: Helmholtz Centre Berlin for Materials and Energy, Hahn-Meitner-Platz, 14109 Berlin, Germany. Tel: +491 30 8062-2079, 8062-2730, 8062-2774  
Email address: [wanderka@helmholtz-berlin.de](mailto:wanderka@helmholtz-berlin.de)

different compositional fluctuations. The results are discussed in terms of species segregation using mixing enthalpy of atom pairs.

**Keywords:** High entropy alloys, TEM/EDX analysis, 3D-AP measurements

## 1. Introduction

The recently developed high entropy (HE) alloys belong to a new class of metallic materials firstly introduced by Yeh [1, 2]. The HE alloy is defined by J.W Yeh as an alloy having at least five principal elements and equiatomic or near equiatomic composition [3, 4]. Less atomic size difference and a near zero value of the absolute enthalpy of mixing facilitate the formation of solid solution for the equi-atomic alloy. The atomic size difference and enthalpy of mixing of constituent in AlCoCrCuFeNi HE alloy is 0.0483 and -4.77 kJ/mol, respectively [5]. Such HE alloys can exhibit high hardness [3] and excellent resistance to softening even at 800°C [6, 7], which make them candidate materials for many potential applications. It is well known that the macroscopic mechanical properties are correlated to the microscopically observed phases of materials. However, only a few studies have been carried out on the microstructure of HE alloys [4, 8, 9]. It was reported that after casting the HE alloys tend to form simple solid solution phases, mainly of fcc or bcc structure [4,8].

The number of the phases formed and their structure depends on the alloying elements in HE alloys synthesized under same processing conditions [8]. For quinary alloys such as CoCrCuFeNi, the formation of only one solid solution, a fcc phase was observed [8]. In contrast, the six element alloy AlCoCrCuFeNi shows the formation of fcc and bcc

phases with a dendritic microstructure [8]. Scanning electron microscopy (SEM) and transmission electron microscopy (TEM) investigations of the dendrites in AlCoCrCuFeNi alloy show a modulated plate structure that was assumed to be formed as a result of spinodal decomposition [3]. The modulated plates are oriented along  $\langle 100 \rangle$  directions of the matrix and are composed of ordered bcc plates (B2 structure) and disordered bcc interplates with the same lattice parameter of 2.89Å but of different chemical compositions [3, 8]. Within the plates, small nm-sized (7 to 50nm) Cu-rich precipitates of fcc structure were also identified [8]. Recently, two phases enriched in Cr-Fe and Ni-Al have been observed in the dendrites [9] upon decomposition. However, the decomposition behaviour of multi-component AlCoCrCuFeNi HE alloy has not been studied so far and needs further investigation.

The present investigation is focused on the study of the decomposition behaviour of a multi-component AlCoCrCuFeNi HE alloy synthesized by the two different processing conditions splat quenching and casting. The splat-quenched and as-cast high entropy AlCoCrCuFeNi alloy was investigated using X-ray diffraction, TEM and three dimensional - atom probe (3D-AP). Especially the 3D-AP measurements were used to map the fine-scale distribution of alloying elements in as-cast high entropy alloy.

## **2. Experimental**

Aluminium, Cobalt, Chromium, Copper, Iron and Nickel of 99.999% purity were used as raw materials for producing HE alloy. This alloy was manufactured in the materials laboratory of the Helmholtz Centre Berlin for Materials and Energy, Germany. The multi-component AlCoCrCuFeNi alloy was produced by levitation melting the

constituent elements in an equiatomic ratio in an induction furnace. The furnace was operated at 10.8 kW with 200 kHz frequency. The levitation melting and casting was performed in pure argon atmosphere. Repeated melting was carried out at least 5 times to improve the chemical homogeneity of the alloy. The ingots were solidified in flowing argon which provided a cooling rate of 10-20 K/s. The solidified ingots were 20 mm in diameter and 20 mm thick and were cut into thin pieces of 2 mm thickness for characterisation. The splats of AlCoCrCuFeNi alloy were produced in vacuum ( $10^{-6}$  mbar) in an electromagnetic levitation (EML) chamber. The splat cooling device allows us to reach quenching rates of the order of  $10^6$ - $10^7$  K/s. The splats produced were 40  $\mu$ m thick.

The splat-quenched and as-cast materials were characterized by different techniques such as XRD, scanning electron microscopy (SEM), TEM and 3D-AP. Thin pieces of both the splats and of the as-cast ingots were mechanically polished with down to 1  $\mu$ m diamond paper for the structure characterization by X-ray diffractometry. XRD spectra were measured with  $\text{CuK}\alpha$  radiation in the  $\theta$ - $2\theta$  configuration using Bruker AXS, D8 diffractometer. Thin-foil specimens suitable for TEM observations were prepared by mechanical thinning down to 20  $\mu$ m thickness followed by Ar-ion milling. The microstructure of the samples was characterized by TEM in a Philips CM30 operated at 300 kV equipped with a Energy Dispersive X-ray (EDX) spectrometer. The beam size in the EDX measurements was usually 10 nm. Thin  $0.2 \times 0.2 \times 10 \text{ mm}^3$  large rods were cut from the ingots for atom probe (3D-AP) measurements. From these rods sharp tips were prepared by polishing in two steps: first by mechanical polishing down to 2  $\mu$ m in diameter using 1  $\mu$ m diamond paper, then by a focused ion beam provided by a ZEISS

1540 EsB cross beam microscope containing SEM & FIB. Tips with a radius below 50 nm were milled by gallium ions of 30 kV energy and a beam current starting with 2000 pA and finishing with 50 pA. The finally prepared sharp tips were checked using TEM as shown in Fig.1. The 3D-AP analysis was performed in vacuum of  $10^{-7}$  Pa at a temperature of about 70K. A pulse fraction of 20 % with a pulse penetration frequency of 1000 Hz was applied in the CAMECA atom probe at HZB. Many tips were investigated from which three important results (namely volume I, II and III) that are representative for the as-cast HE alloy are presented here.

Nanohardness and indentation elastic modulus of the splat-quenched and as-cast high entropy alloys were measured using a Fischer Picodentor HM500. The measurement was carried out at a load of 300 mN for 20 sec. For comparison, the micro hardness of as-cast high entropy alloy was also measured using a Reichert-Jung micro hardness tester MHT-10 applying a load of 890 N for 10 sec.

### **3. Results**

Fig. 2 compares the X-ray diffraction pattern of splat-quenched and as-cast equiatomic AlCoCrCuFeNi high entropy alloy. In the splat-quenched material X-ray diffraction peaks corresponding to a single bcc phase are observed. The formation of a single bcc phase in equiatomic AlCoCrCuFeNi HE alloy has not been reported previously. The lattice parameter of the bcc phase is 2.867Å. Incontrast, in the as-cast alloy Bragg peaks corresponding to two fcc and one bcc structure are observed. The intensity of the diffraction peaks of the bcc phase is much stronger than that of fcc phase which indicates a higher volume fraction of bcc phase than fcc phase in the present alloy. The

magnified image of the diffraction pattern at  $2\theta = 43-44^\circ$  (inset of Fig. 2) shows two peaks, that correspond to two fcc phases named fcc1 and fcc2 with different lattice parameters.

The bright field TEM image of splat-quenched HE alloy in Fig. 3 (a) shows the typical microstructure of a polycrystalline material with distinct grain boundaries and grain sizes around  $1.5 \mu\text{m}$ . The dark field TEM micrograph in Fig. 3 (b) imaged using the [001] superlattice reflection reveals small ordered regions (bright contrast) of a few nm diameter. The corresponding [100] zone axis diffraction pattern (inset of Fig. 3 (b)) proves the presence of a ordered bcc structure.

Fig. 4 shows bright field TEM micrographs of the as-cast HE alloy. The as-cast alloy solidifies dendritically and is embedded in an interdendritic matrix, see Fig. 4 (a). Several typical precipitate morphologies within the dendrites are shown in the TEM bright-field image in Fig. 4 (b). The [001] zone axis diffraction pattern (inset of Fig. 4 (b)) displays the superlattice reflections generated by the ordered B2 precipitates. Plate-like precipitates with a dark contrast having a thickness of about 50 nm and a length of 200-500 nm are aligned along the  $\langle 110 \rangle$  matrix direction. The plate-like precipitates are coherent with the bcc solid solution matrix. Weak streaks in the corresponding selected area electron diffraction (SAED) pattern are visible that arise from the plate-like precipitates. The lattice parameter of the bcc phase as measured from SAED is  $2.879 \text{ \AA}$ . Small and almost spherical precipitates with a size of 5-15 nm are also present. Beside the plate-like and the spherical precipitates in the dendrites, some regions with rhombohedron-shaped are also detected (Fig. 4 (c)). The corresponding SAED of this

phase is shown in the inset. The  $\langle 110 \rangle$  zone axis exhibits superlattice reflections which corresponds to an ordered  $L1_2$  structure. The edges of the rhombohedron-shaped phases are aligned along  $\langle 111 \rangle$  directions. The lattice parameter of about 3.639 Å of the phase as determined by SAED corresponds to the fcc2 phase as mentioned in Fig. 2. The bright-field TEM image of the interdendritic region is shown in Fig. 4 (d). The corresponding SAED pattern is shown in the inset. The  $\langle 112 \rangle$  zone axis of diffraction image clearly reveals that the interdendritic region belongs to the phase with fcc structure. Weak superlattice reflections corresponding to a  $L1_2$  structure are also visible. The lattice parameter of the interdendritic phase as measured by SAED is about 3.583 Å and is close to the fcc1 phase measured by X-ray diffraction, see Fig. 2.

The chemical compositions of the splat-quenched (Fig. 3) and as-cast high entropy alloys (Fig. 4, marked by A, B, C, D, E and F regions) were estimated by EDX analysis in the TEM and are listed in Table 1. The splat-quenched sample shows a homogeneous distribution of elements and is close to equiatomic composition. However, the concentration of Al is less than that of other elements. In the as-cast high entropy alloy the dendrites contain plates enriched in Al-Ni (A) or Ni (C) and inter-plates enriched in Cr-Fe (B). The plate-like precipitate (D), spherical precipitate, rhombohedron-shaped phases (E) and interdendrite region (F) are Cu-rich phases but of different compositions. Both the plate-like precipitates and the spherical precipitates contain more than 84 at. % Cu.

The microchemical information of the phases present in the dendrites of as-cast HE alloy was obtained by 3D-AP tomography with nearly atomic resolution (Fig. 5-10).

Fig. 5 displays the three dimensional reconstruction of Al, Cr, Ni, Co, Fe and Cu atom positions in an analyzed volume of  $9.5 \times 9.5 \times 93 \text{ nm}^3$  (volume I). All the alloying elements in the HE alloy are non-uniformly distributed and form three discrete regions. The compositions of these regions were determined from concentration depth profiles using a cylinder of 1 nm radius located in the middle through out the analyzed volume. A cylinder of 1 nm radius was selected in order to reveal the sharp change in the concentration gradient at the interface. The concentration depth profiles in Fig. 6 demonstrate that region 1 is mainly enriched in Al and Ni. Region 2 is enriched in Cr and Fe and region 3 is largely enriched in copper. Cobalt is homogeneously distributed in regions 1 and 2 but depleted in region 3. In region 1, small Cu-rich precipitates can also be found. The concentration depth profiles of small (about 2 nm in size) copper precipitate was reconstructed by taking a cylinder of 1 nm radius perpendicular to one side of the precipitate / matrix interface, see Fig. 7. The interface of the Cu-rich precipitate is very sharp and about 0.5 nm wide. The small precipitate was observed to contain more than 88 at% Cu (see also Table 1, 1a). The transition interface between the Al-Ni rich and Cr-Fe rich region is comparably broad (about 8 nm) as observed in the depth profile in Fig. 6.

The compositional fluctuations of elements in between two Cu-rich precipitates can be observed by concentration depth profiles taken along the axis of the cylinder of 1 nm radius in another volume (volume II) and is displayed in Fig. 8. The cylinder cuts out a region with alternating enriched and depleted Al-Ni and Cr-Fe areas. The width of the Al-Ni enriched areas is approximately 5 and 10 nm, while the Cr-Fe rich regions are 20 and 35 nm thick. The composition of Co in both areas is almost the same. However, Cr,



Fe and Co in Cr-Fe rich areas are not distributed homogeneously. Moreover, compositional fluctuations of Cr are observed that are anti-correlated to Fe and Co. The average chemical compositions of Al-Ni rich and Cr-Fe rich areas are similar to the corresponding areas observed in Fig. 6 and therefore they will not be additionally numbered and included in the Table 1.

Fig. 9 displays another example of 3D-AP measurements (volume III). The 3 dimensional reconstructions of Al, Cr, Ni, Co, Fe and Cu atom positions are shown in an analyzed volume of  $12.6 \times 12.6 \times 134.2 \text{ nm}^3$ . A general observation of this volume shows two discrete regions that are enriched and depleted in Cr. Only at first sight all other elements seem to be homogeneously distributed throughout the analyzed volume. A quantitative analysis of concentration depth profiles reveals an inhomogeneous distribution of all the alloying elements. The depth of 134 nm in Fig. 10 is subdivided into 4 regions. In order to keep the numbers of the regions consistent (Table 1) with the previously numbered regions, the regions of Fig. 10 are numbered with 4, 5, 6, and 7. Region 4 is enriched in Al, Ni, Fe and depleted in Cr, Co and Cu. However, within this region after a depth of around 20 nm a small fluctuation in Cu is observed that corresponds to the Cu-rich precipitate. Region 5 is enriched in Ni, Cr and Fe. It seems that the core of this area contains equal amounts of Ni, Cr and Fe and the boundary is enriched with Ni. Region 6 shows a large gradient in Ni and Co concentrations, whereas Al, Fe, Co and Cu are homogeneously distributed. The concentrations of Cu and Al in regions 6 and 7 are less than the nominal values. Accordingly, in region 7 the amount of Ni, Fe, Cr and Co is higher than their nominal composition. The local concentrations of regions 4 to 7 are also listed in Table 1. All regions whose chemical compositions

deviate from the homogeneous distribution of elements (16.67 at. %) are listed in Table 1. The error bars for the chemical composition of the elements are represented by  $2\sigma$  standard deviation, determined by standard counting statistics. The compositions of regions 1 (Al-Ni), 2 (Fe-Cr) and 3 (Cu-rich) can be identified as regions marked A, B and D in Fig. 4, respectively.

Hardness and indentation elastic modulus of the splat-quenched and as cast high entropy alloy are given in Table 2. From this table it is observed that the hardness of splat-quenched (539 HV) and as-cast (534 HV) alloy is almost equal. However, the indentation elastic modulus of as-cast material (182 GPa) is markedly higher than that of splat-quenched material (105 GPa).

#### **4. Discussion**

The successful preparation of a cubic bcc phase AlCoCrCuFeNi HE alloy by rapid cooling ( $10^6$ - $10^7$  K/s) is reported in the present work for the first time. The high cooling rates during splat quenching prevents the normal process of nucleation and growth of equilibrium phases and hence metastable solid solutions can be obtained as predicted in [10]. However, the single bcc phase obtained from both XRD (Fig. 2) and TEM (Fig. 3) shows the presence of small ordered regions (Fig. 3 (b)) which indicates an initial stage of phase decomposition already during solidification. According to these observations the velocity of the phase boundary between the precipitating and growing phases in melt is more than that of atomic diffusion velocity [11]. Therefore, the proposed idea that HE alloys form random nanostructured solid solution phases during solidification [12, 13] can be supported by this study.

The decomposition of a supersaturated solid solution takes place at lower cooling rates (10-20 K/s) and results in strong phase separation as observed in the as-cast alloy (Fig. 4). The volume fraction of the bcc phase in the as-cast alloy is more than that of the fcc phase (Fig. 2). The splat-quenched sample also shows the formation of a single bcc phase (Fig. 2). We can conclude that the matrix of AlCoCrCuFeNi high entropy alloy is the bcc phase, while the other phases form by decomposition. In summary, six phases were observed in the as-cast material (Fig. 4): the interdendritic region consists of fcc-L1<sub>2</sub> phase and dendrites contain spherical Cu-rich precipitates, plate-like precipitate of B2 type, rhombohedron-shaped precipitates of L1<sub>2</sub> type, Al-Ni rich plates (B2) and Cr-Fe rich interplates (bcc). However, the number of phases is only one less than the maximum number permitted in equilibrium according to Gibb's phase rule [14]. The presence of fcc2 (Cu-rich, rhombohedron-shaped) phase for AlCoCrCuFeNi alloy has not been reported previously [4, 8].

The microstructural studies show that Cu is the element that separates first and forms Cu-rich phases (Table 1). The behaviour of Cu can be explained by its strong repulsive interaction with the other elements and is not surprising, since Cu has the highest positive mixing enthalpy with Fe, Cr, Co and Ni [15]. The composition of the Cu-rich plate-like precipitate as given in Table 1, indicate that they consist of Cu (83 to 85 at.%) with small amounts of Al (4 to 8) and Ni (4 to 5), which is in good agreement with an ordered bcc (B2) phase (82-86%Cu, 10.5-14%Al, 3-5 % Ni) observed during quenching of Cu-Ni-Al [16]. Therefore, it is concluded that the plate-like precipitates have a B2 structure. Both types of Cu-rich precipitates are exclusively observed in the Al-Ni rich

region and not in Cr-Fe rich regions which is in accordance with the recent literature [8-9]. This may be due to its negative enthalpy of mixing with Al (Table 3).

The detailed investigations of the local concentration within the dendrites point at alternating regions enriched or depleted in Ni-Al or Cr-Fe (see Table 1, regions 1 and 2). The wavelengths of these fluctuations (information from several 3D-AP measurements) range from 5 to 45 nm (Fig. 6 and Fig. 8). Areas with similar compositions were also observed using TEM/EDX microanalysis (Table 1, regions A and B). The presence of ( $\alpha$ -Fe, Cr) solid solution and Ni-Al intermetallic phases in the same HE alloy was recently also reported [9]. However, the wavelengths of Ni-Al and Cr-Fe rich regions reported in the EDS line scan analysis [9] are much larger than the fluctuations obtained in the present work. This is because of the non-uniformity in size and distribution of phases in as-cast material.

The formation of the NiAl phase can also be explained by the largest negative mixing enthalpy which is -22 kJ/mol (see Table 3) [15]. However, this phase consists of large amounts of Co, Fe, Cu and Cr. Based on the local concentration analysis of the atom probe and on the data reported in the literature [17], it can be assumed that Fe prefers the Al sites whereas Cr and Co prefers the Ni sites in the NiAl phase. Thus, the stoichiometry of the NiAl phase could be  $(\text{Ni}_{28}\text{Co}_{19}\text{Cr}_3)(\text{Al}_{30}\text{Fe}_{12}\text{Cu}_8)$ .

As seen in Table 3 the mixing enthalpy of a Cr – Fe pair is just -1 kJ/mol [15].

Nevertheless, they segregate together in the Cr-Fe rich region. The detailed analysis of the atom probe data shows that Cr and Fe fluctuations are anti-correlated (Fig. 6 and

Fig. 8). The amplitude of Cr fluctuations in the Cr-Fe rich regions lies in the range of 32-47 at.% and the wavelength is about 6 nm (Fig. 8). The fluctuations of Cr and Fe in a Fe-Cr-Co based alloy have been previously investigated in detail [18]. Fe-Cr-Co-based alloys belong to the permanent magnets and the magnetic hardening of this alloy was explained to be associated with the modulated structure formed by spinodal decomposition. The amplitude of element fluctuations in the present investigations is much lower than in [18], but the same tendency of element correlation is obtained indicating decomposition of Cr-Fe phase in the as-cast alloy.

Regions enriched in Al-Ni-Fe (Fig. 10, region 4) can also be explained by the negative mixing enthalpy of Al - Ni pairs and Al - Fe (-11 kJ/mol) [15] pairs which are large enough for clustering. The composition of the Al-Ni-Fe phase (Table 1) is similar to the composition of the ordered bcc (B2) phase recently reported in maraging steels [19]. Such Al-Ni-Fe fluctuations obtained in this study could act as nuclei for the crystallisation of intermetallic phases during heat treatment.

From the results obtained in the present study it cannot be confirmed that in HE alloys all elements can be regarded as solute or solvent and are expected to be randomly distributed in the crystal lattice, according to the statistically expected occupancy [13]. Moreover, it is shown that only high mixing entropy leads to the formation of phases with simple cubic crystal structure in both the solid solution (splat-quenched state) and also upon decomposition in the as-cast HE alloy.

The indentation elastic modulus of as-cast high entropy alloy is much higher than that of splat-quenched alloy. The mechanical property of the alloys is known to depend on the microstructure. Therefore, the result of the present investigations is not unexpected as the splat-quenched alloy shows almost homogeneous distribution of elements whereas the as-cast alloy shows later stage of phase decomposition with coarse microstructure.

### **Summary**

The overall process of decomposition of supersaturated solid solution, formation of precipitates and phase segregation observed during solidification of a AlCoCrCuFeNi HE alloy at two different cooling rates is presented schematically in Fig. 11. Splat-quenching (cooling rate  $10^6$ - $10^7$  K/s) leads to the formation of bcc ordered phase. In contrast production of alloy at cooling rates of 10-20 K/s leads to phase separation into six phases with bcc and fcc structure. High entropy alloy synthesized with elements containing large differences in enthalpy of mixing such as Al-Ni, Cu-Ni and Fe-Cr leads to segregation during solidification. The preferential segregation of elements is explained on the basis of mixing enthalpies.

### **References**

- [1] Ranganathan S. *Current Sci* 2003;85:1404
- [2] Yeh JW. *Knowledge Bridge* 2003;40:1
- [3] Yeh JW, Chen SK, Lin SJ, Gan JY, Chin TS, Shun TT, Tsau CH, Chang SY. *Adv Engg Mater* 2004;6:299
- [4] Tung CC, Yeh JW, Shun TT, Chen SK, Huang YS, Chen HC. *Mater Lett* 2007;61:1

- [5] Zhang Y, Zhou Y J, Lin JP, GL Chen, PK Liaw. *Adv Engg Mater* 2008;10:534
- [6] Tong CJ, Chen MR, Chen SK, Yeh JW, Shun TT, Lin SJ, Chang SY. *Metall Mater Trans* 2005;36A:1263
- [7] Yeh JW, Chen YL, Lin SJ, Chen SK. *Mater Sci Forum* 2007;560:1
- [8] Tong CJ, Chen YL, Chen SK, Yeh JW, Shun TT, Tsau CH, Lin SJ, Chang SY. *Metall Mater Trans* 2005;36A:881
- [9] Wang YP, Li BS, Fu HZ. *Adv Engg Mater* 2009;11:641
- [10] Duwez P, Willens RH, Klement W. *J Appl Phys* 1960;31:1136
- [11] Galenko P, Jou D. *Physica A* 2009; 388:3113
- [12] Wang YP, Li BS, Ren MX, Yang C, Fu HZ. *Mater Sci Engg A* 2008;491:154
- [13] Yeh JW, Chen SK, Gan JY, Lin SJ, Chin TS, Shun TT, Tsau CH, Chang SY. *Metall Mater Trans* 2004;35A:2533
- [14] Li A, Zhang Xi. *Acta Metallurg Sinica* 2009;22:219
- [15] Takeuchi A, Inoue A. *Mater Trans* 2005;46:2817
- [16] Keshari AK, Singh P, Chakkingal U, *Proceeding of International Symposium of Research Students on Materials Science & Engineering, December 2004, Chennai India.*  
Pp1-7
- [17] Wanderka N, Glatzel U. *Mater Sci Engg A* 1995;203:69
- [18] Zhu F, Wendt H, Haasen P. *Scripta Met* 1982;18:1175
- [19] Höring S, Wanderka N, Banhart J. *Ultramicroscopy* 2009;109:574

## Figure Captions

**Fig. 1** Bright field TEM image of a sharp tip prepared from as-cast HE alloy in two steps: mechanical polishing and subsequent sharpening using focussed ion beam (FIB).

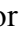



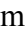

**Fig. 2** X-ray diffraction patterns showing comparison between splat-quenched and as-cast equiatomic AlCoCrCuFeNi high entropy alloys. The splat-quenched HE alloy shows the presence of a single bcc phase ( $a_{\text{bcc}}=2.867\text{\AA}$ ), whereas the as-cast HE alloy indicates the presence of one bcc ( $a_{\text{bcc}}=2.866\text{\AA}$ ) and two fcc phases. Two fcc phases are clearly visible from two overlapping peaks shown in the inset, corresponding to the two  $\{111\}$  planes with slightly different lattice parameters ( $a_{\text{fcc1}}=3.594\text{\AA}$  and  $a_{\text{fcc2}}=3.619\text{\AA}$ ).

**Fig. 3** TEM images of the splat-quenched equiatomic AlCoCrCuFeNi HE alloy: a) Bright field image showing polycrystalline structure; b) Dark field micrograph of microstructure imaged by  $[001]$  superlattice reflection shows regions with different contrast on the scale of a few nm. The corresponding diffraction pattern in the  $[100]$  zone axis indicates a partially ordered bcc phase with B2 structure ( $a_{\text{bcc}}=2.873\text{\AA}$ ).

**Fig. 4** Bright-field TEM images of as-cast equiatomic AlCoCrCuFeNi HE alloy: a) dendrite and interdendritic regions; b) Microstructure of dendritic region with plate-like precipitates oriented along the  $\langle 110 \rangle$  directions. The corresponding electron diffraction pattern of  $[001]$  zone axis presented in the inset exhibits reflections of ordered bcc, B2 structure ( $a_{\text{bcc}}=2.879\text{\AA}$ ). The characters A, B, C and D are positions of the EDX analyse; c) dendritic region with rhombohedron-shaped phases ( $a_{\text{fcc2}}=3.639$ ). The







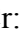

corresponding electron diffraction pattern of the  $\langle 110 \rangle$  zone axis in the inset displays superlattice reflexions of an ordered fcc phase; d) Microstructure of the interdendritic region and corresponding electron diffraction pattern of the  $\langle 112 \rangle$  zone axis, showing superlattice reflexions of the ordered fcc phase ( $a_{\text{fcc}} = 3.583 \text{ \AA}$ ).

**Fig. 5** Three dimensional reconstruction of Al, Cr, Ni, Co, Fe and Cu atom positions in an analyzed volume  $9.5 \times 9.5 \times 93 \text{ nm}^3$  (volume I) of as-cast AlCoCrCuFeNi high entropy alloy. The symbols for different atoms are Al: , Co: , Cr: , Cu: , Fe:  and Ni: .

**Fig. 6** Concentration depth profiles of all alloying elements in as-cast AlCoCrCuFeNi high entropy alloys in an analysed volume  $9.5 \times 9.5 \times 93 \text{ nm}^3$  (volume I). The dotted lines separate regions 1, 2 and 3 enriched in Al-Ni, Cr-Fe and Cu, respectively.

**Fig. 7** Concentration depth profiles through a small Cu precipitate observed in the Al-Ni rich area (volume I, region 1a).

**Fig. 8** Concentration depth profiles of all alloying elements in as-cast AlCoCrCuFeNi high entropy alloys in an analysed volume  $9.5 \times 9.5 \times 74 \text{ nm}^3$  (volume II). Regions enriched in Al-Ni and Cr-Fe are visible. Cu-rich precipitates are located both at right and left side of the measurement.

**Fig. 9** Three dimensional reconstruction of Al, Cr, Ni, Co, Fe and Cu atom positions in an analyzed volume  $12.6 \times 12.6 \times 134.2 \text{ nm}^3$  (volume III) of as-cast AlCoCrCuFeNi high entropy alloy. The symbols used for different atoms are Al: , Co: , Cr: , Cu: , Fe:  and Ni: .

**Fig. 10** Concentration depth profiles of all alloying elements in AlCoCrCuFeNi high entropy alloy (volume III, data set from Fig.9). The dotted lines separate the region 4, 5, 6 and 7 enriched in Al-Ni-Fe, Ni-Cr-Fe, CrFe(NiCo), Ni-Cr-Co-Fe, respectively.

**Fig. 11** Schematic representation of phase segregation observed during cooling of AlCoCrCuFeNi high entropy alloy by two different processing conditions: splat quenching (cooling rate  $10^6$ - $10^7$  K/s) and casting (cooling rate 10-20 K/s).

### **Table Captions**

**Table1.** Crystal structure and chemical composition (in at.%) of splat-quenched and as-cast HE alloys. The compositions of polycrystalline grains in splat-quenched alloy and different phases marked in as-cast alloy (regions A-F as marked in Fig. 4) are measured by EDX/TEM. The local concentrations of region 1-7 (defined in Fig.'s 6,7 and 10) are measured by 3D-AP. The error in concentration is represented by  $2\sigma$  standard deviation.

**Table2.** Hardness and indentation elastic modulus values of the splat-quenched and as-cast HE alloy.

**Table3.** Enthalpy of mixing (kJ/mol) of unlike atom pair consisting of elements in AlCoCrCuFeNi estimated in [15].

**Table1.**

<b>Symbols</b>	<b>Regions enriched</b>	<b>Crystal structure</b>	<b>Al</b>	<b>Co</b>	<b>Cr</b>	<b>Cu</b>	<b>Fe</b>	<b>Ni</b>
Splat- quenched	Grains	B2	13.1±3	17.7±3	16.2±3	18.7±3	17.6±3	16.7±3
As-cast	<b>Dendrite</b>							
A	Al-Ni	B2	25.8 ±3	17.9±3	3.0±3	10.4±3	12.1±3	30.8±3
B	Cr-Fe	bcc	2.2±3	20±3	43.2±3	0.3±3	29±3	5.3±3
C	Ni	B2	19.4±3	19.5±3	6.3±3	10±3	14.4±3	30.4±3
D	Plate precipitate	B2	4.9±3	1.8±3	1.1±3	85±3	2.0±3	5.2±3
E	Rhombohedral- shaped phases	L1 <sub>2</sub>	8.0±3	8.9±3	2.7±3	58.8±3	6.6±3	15±3
1	Al-Ni	B2	29.7±1.5	18.4±1.3	2.5±0.5	8.6±0.9	12.7±1.1	28.1±1.5
1a	Spherical precipitate		4.3±1.4	0.6±0.9	0.01±0.3	88.5±1.6	2.5±0.9	4.1±1.5
2	Cr-Fe	bcc	2.8±0.6	18.8±1.2	39.6±1.4	1.3±0.4	31.3±1.4	6.2±0.5
3	Plate precipitate	B2	7.8±0.7	1.9±0.4	0.5±0.1	83.5±1.0	1.1±0.2	5.2±0.6
4	Al-Ni-Fe		31.2±1.6	6.5±0.8	3.3±0.6	7.9±1.0	25.6±1.5	25.5±1.5
5	Ni- Cr-Fe		1.5±1.0	4.9±1.8	28.4±3.7	4±1.4	29.3±3.9	31.9±3.7
6	CrFe(NiCo)		6.3±0.9	10.5±1.1	21.9±1.5	4.9±0.8	23.4±1.5	33±1.7
7	Ni-Cr-Co-Fe		7.4±0.7	21.1±1.1	19±1.0	5.5±0.6	22.8±1.1	24.2±1.2
	<b>Interdendritic region</b>							
F	Cu	L1 <sub>2</sub>	7±3	2.9±3	1.3±3	77.1±3	2.5±3	9.1±3

**Table2.**

Materials	Microhardness (HV)	Nanohardness (HV)	Elastic modulus GPa
Splat-quenched		539	105
As-cast	500	534	182

**Table3.**

▲H mix→ Elements↓	Ni	Cr	Al	Co	Fe
Cu	4	12	-1	6	13
Ni		-7	-22	0	-2
Cr			-10	-4	-1
Al				-19	-11
Co					-1

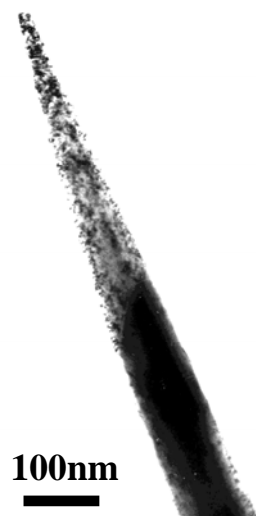


Fig. 1.

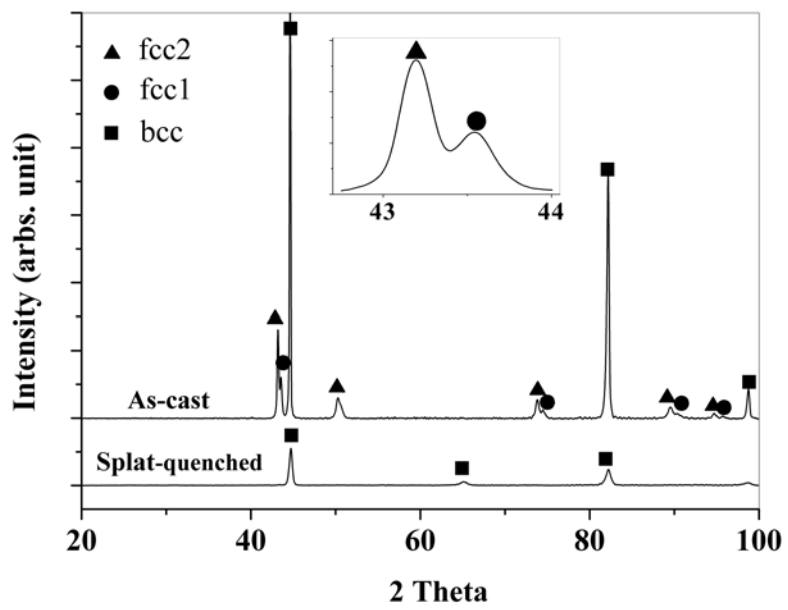
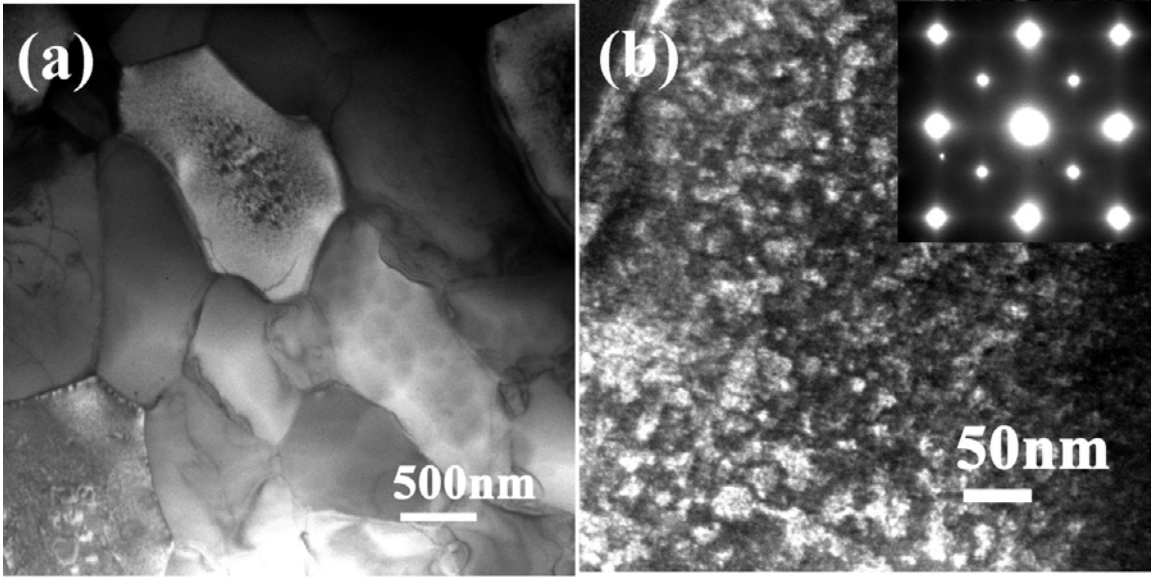
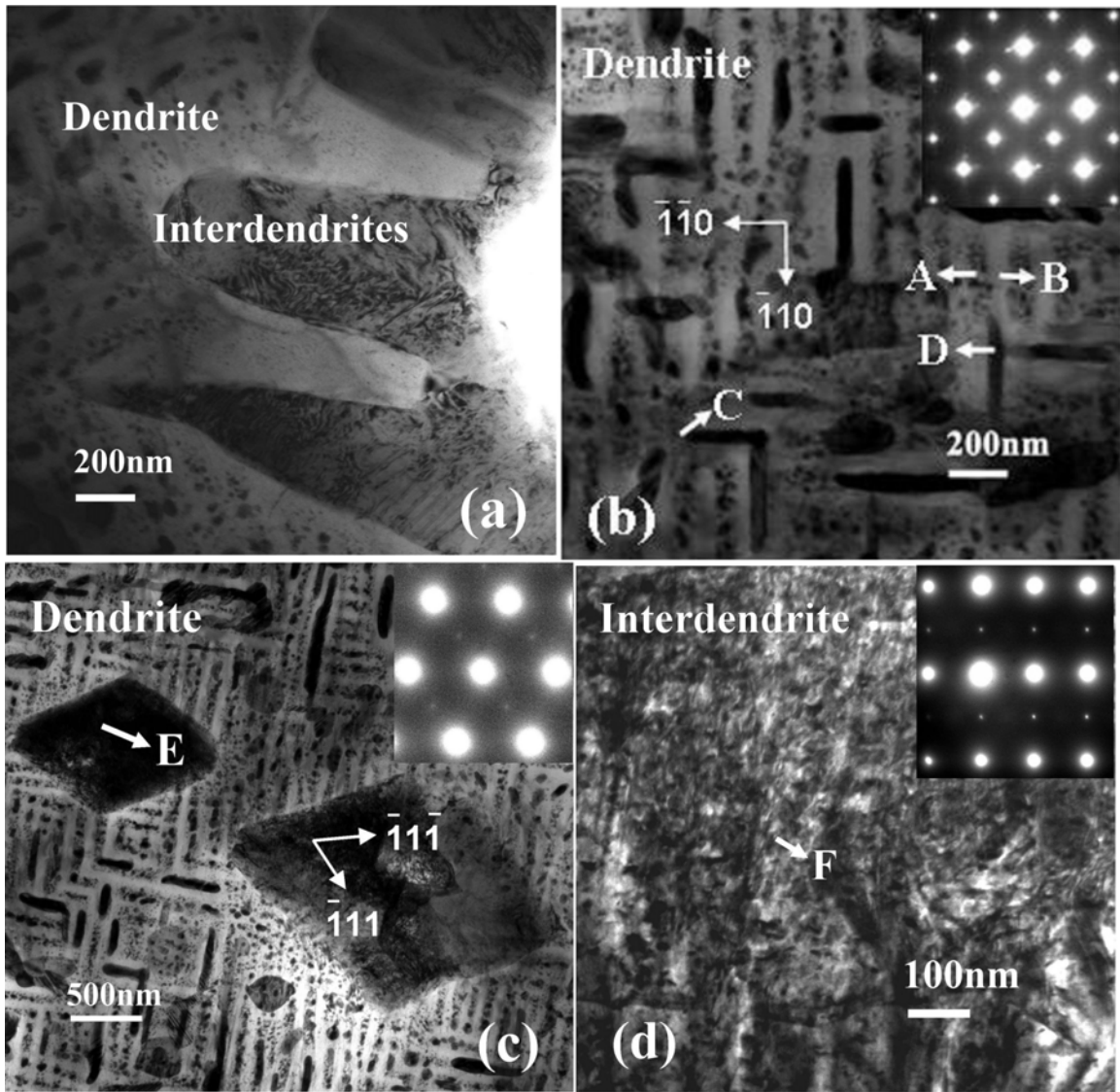


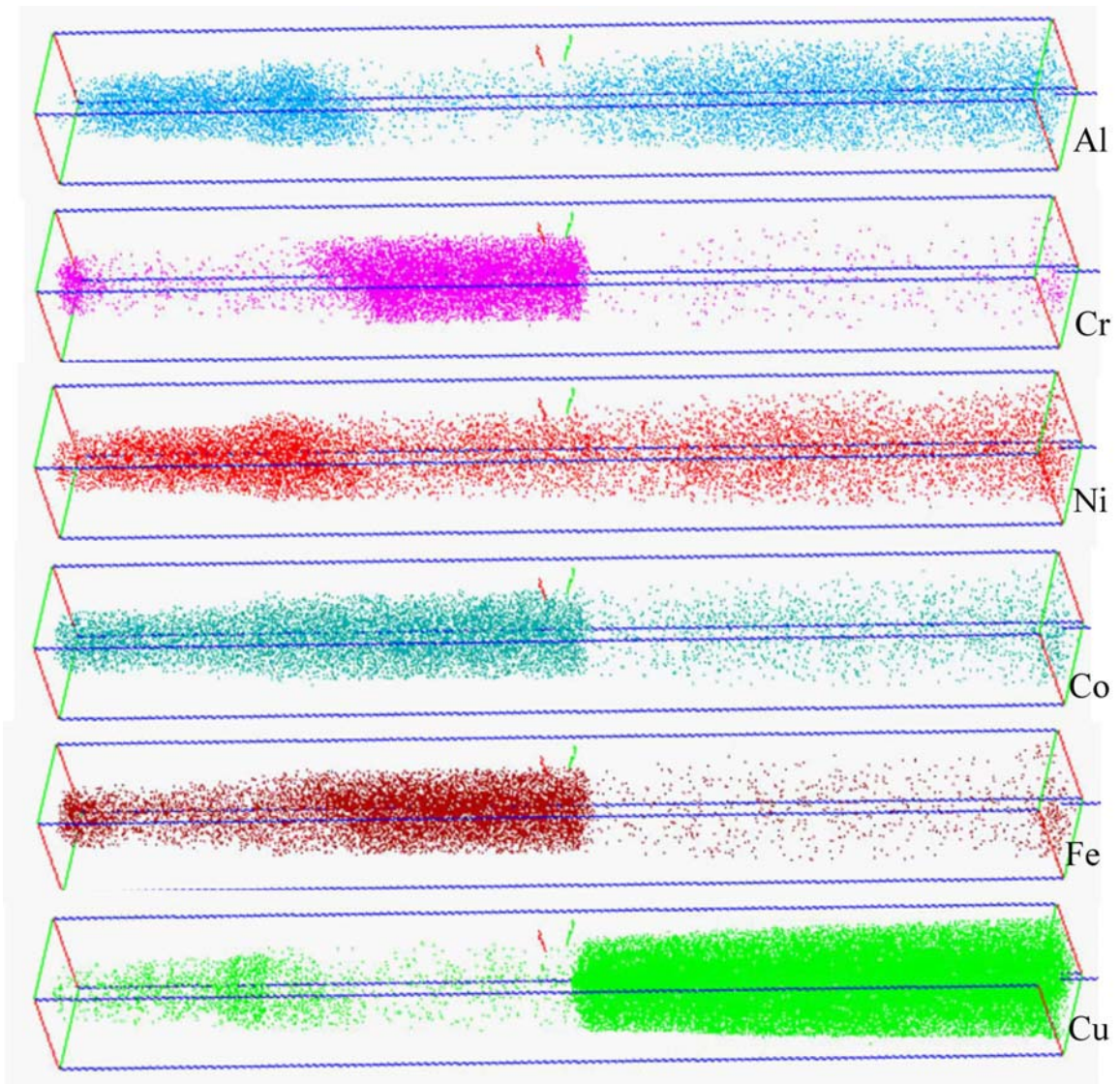
Fig. 2.



**Fig. 3.**



**Fig. 4.**



**Fig. 5.**



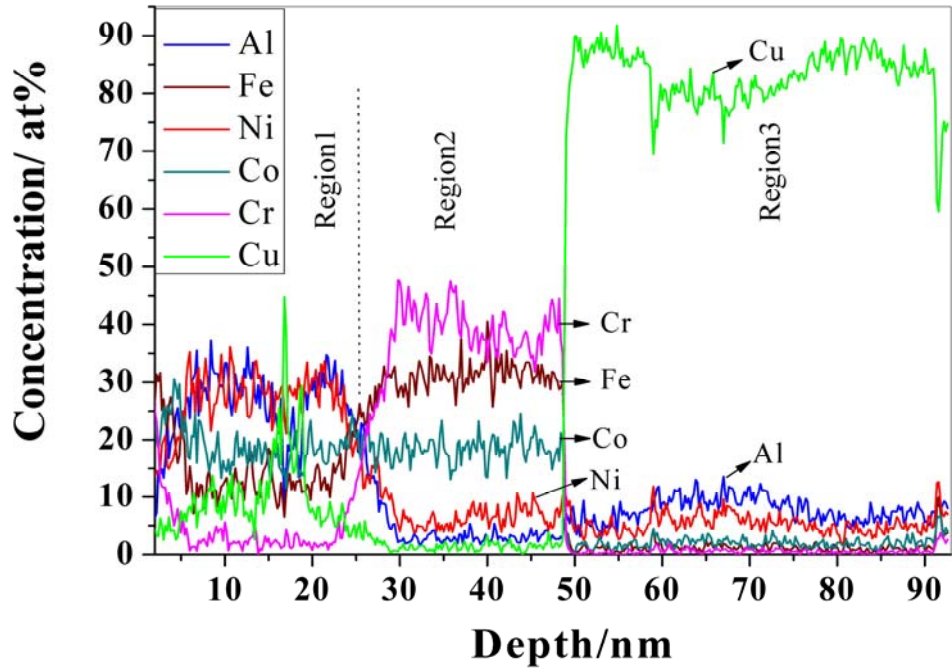


Fig. 6.

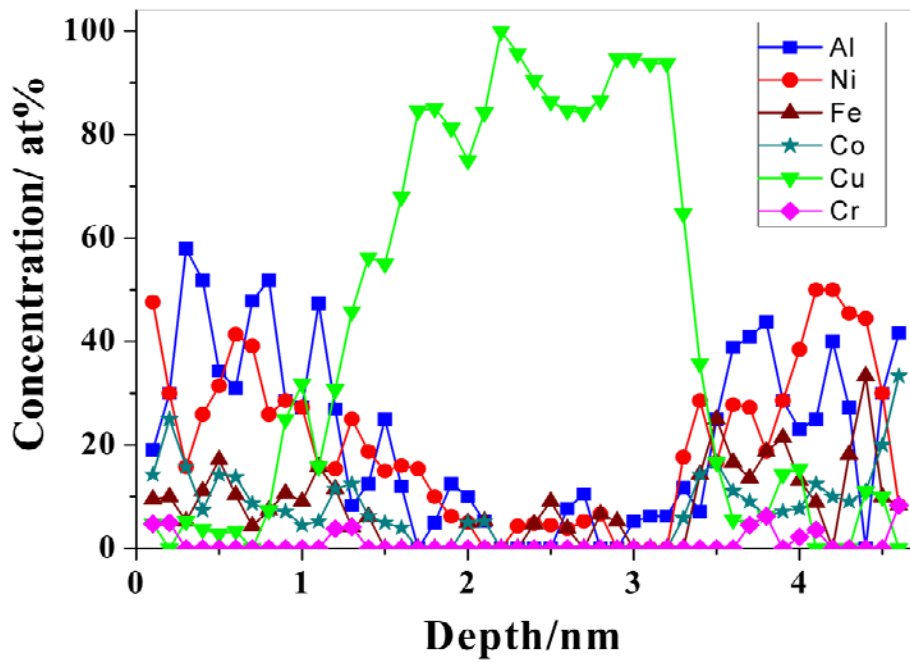


Fig. 7.

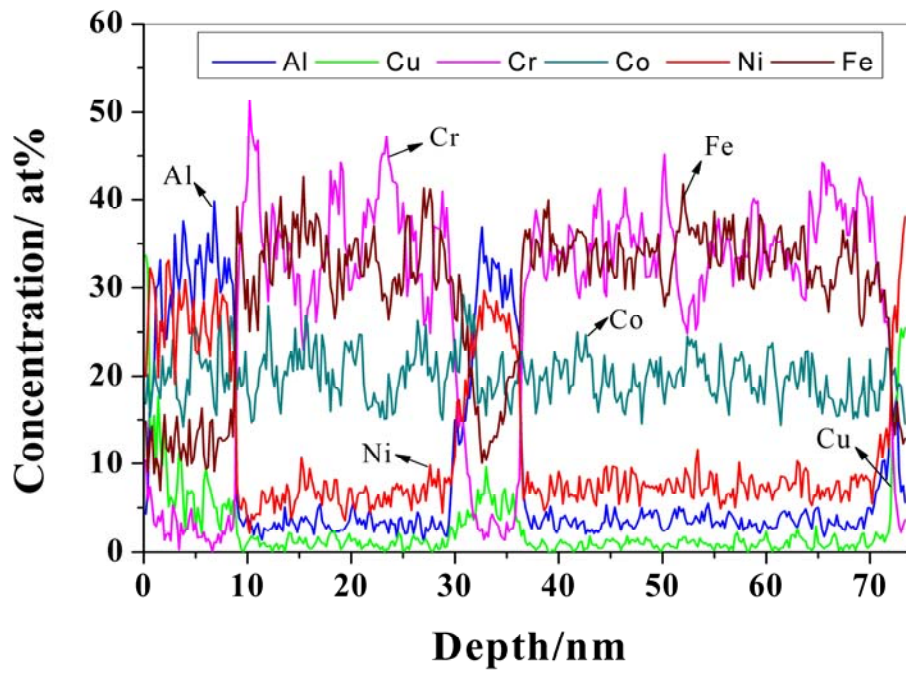
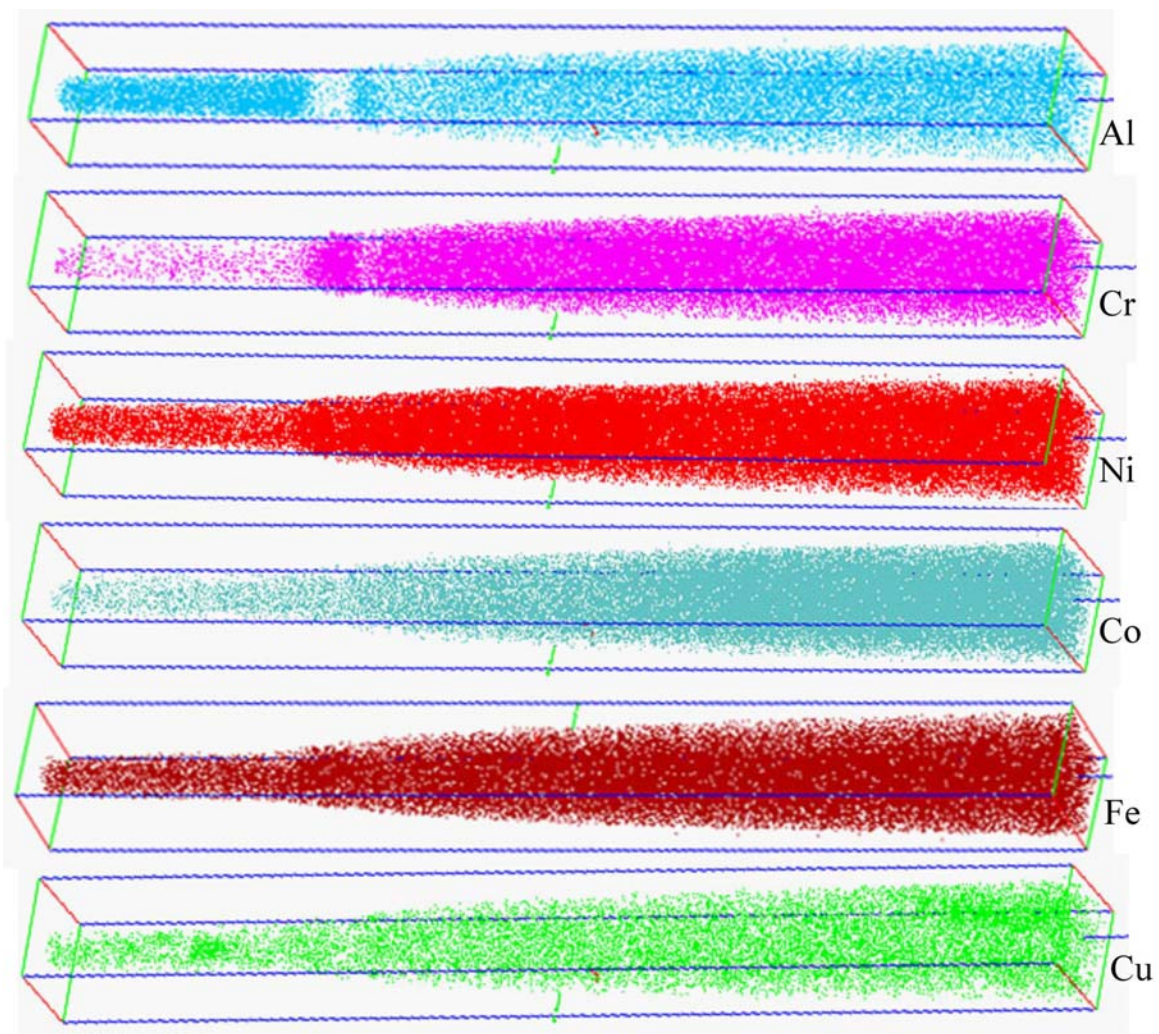


Fig. 8.



**Fig. 9.**

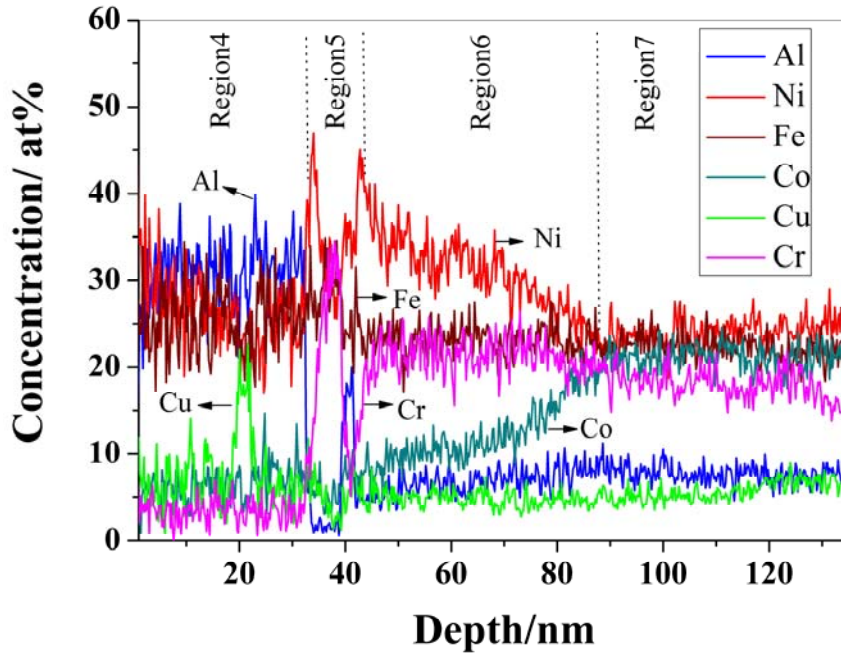


Fig. 10.

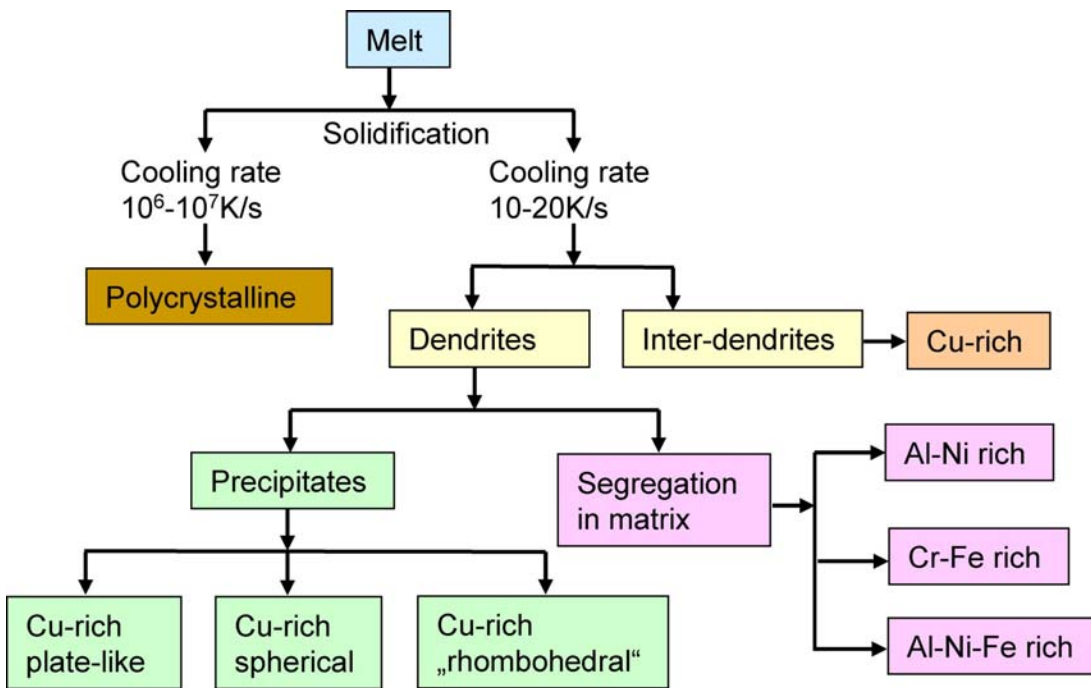


Fig. 11.